ADVANCED ENERGY MATERIALS
www.advenergymat.de

Field Effect versus Driving Force: Charge Generation in Small-Molecule Organic Solar Cells

Vasileios C. Nikolis, Yifan Dong, Jonas Kublitski, Johannes Benduhn, Xijia Zheng, Chengye Huang, A. Celil Yüzer, Mine Ince, Donato Spoltore, James R. Durrant, Artem A. Bakulin,* and Koen Vandewal**

Efficient charge generation in organic semiconductors usually requires an interface with an energetic gradient between an electron donor and an electron acceptor in order to dissociate the photogenerated excitons. However, single-component organic solar cells based on chloroboron subnaphthalocyanine (SubNc) have been reported to provide considerable photocurrents despite the absence of an energy gradient at the interface with an acceptor. In this work, it is shown that this is not due to direct free carrier generation upon illumination of SubNc, but due to a field-assisted exciton dissociation mechanism specific to the device configuration. Subsequently, the implications of this effect in bilayer organic solar cells with SubNc as the donor are demonstrated, showing that the external and internal quantum efficiencies in such cells are independent of the donor-acceptor interface energetics. This previously unexplored mechanism results in efficient photocurrent generation even though the driving force is minimized and the open-circuit voltage is maximized.

1. Introduction

Due to the low dielectric constants of organic semiconductors, photon absorption by these materials typically results in a tightly bound electron-hole pair (exciton) whose binding energy greatly exceeds the thermal energy. As a result, the dissociation of excitons usually requires the presence of an energetic offset between two molecules, which act as electron donor (D) and electron acceptor (A).[1,2] Exciton dissociation in a mixture of two such molecules yields electron-hole pairs at the D–A interface, often referred to as charge-transfer states (CT states).[3] Charge generation via CT states has been thoroughly studied for OSCs and found to occur with high quantum efficiencies when a sufficient offset exists between the lowest exciton energy (E_{opt}) and the energy of the CT state (E_{CT}), namely the driving force.[4–6] As the field of OSCs now moves towards efficient non-fullerene based D–A systems with low voltage losses, surprisingly high external quantum efficiencies (EQEs) are observed even in the absence of a considerable driving force.[7–11] For a number of such D–A systems, it has been shown that the field induced by the presence of electrodes assists the charge generation mechanism.[12,13] This calls for a re-evaluation of charge generation mechanisms in new materials and systems, including the effects of the external field, delocalization, entropy, and driving force.[7,14]

Single-component OSCs (SCOSCs) promise a simpler device fabrication and a potential solution to the morphological instability of many bulk heterojunction OSCs.[15] SCOSCs do not rely on charge separation at a heterojunction and vivid research has been performed to enhance in the efficiency of those systems by increasing their dielectric constant, exploiting bulk ionization effects or utilizing block copolymers that combine donor and acceptor moieties to facilitate the dissociation of excitons.[16–18] Among others, Chandran et al. have reported the direct free carrier generation in SCOSCs employing the small molecule chloroboron subnaphthalocyanine (SubNc), which reached an EQE of 22% despite the absence of an acceptor molecule.[19] Extending this concept, a two-layer device with chloroboron subphthalocyanine (SubPc) positioned adjacently to SubNc reached an EQE of 50%, although SubNc and SubPc do not form a charge generating type-II heterojunction,

V. C. Nikolis,[+] J. Kublitski, Dr. J. Benduhn, Dr. D. Spoltore
Dresden Integrated Center for Applied Physics and Photonic Materials (IAPP) and Institute for Applied Physics
Technische Universität Dresden
Nöthnitzer Str. 61, Dresden 01187, Germany
E-mail: vasileios_christos.nikolis1@tu-dresden.de
Y. Dong, X. Zheng, C. Huang, Prof. J. R. Durrant, Dr. A. A. Bakulin
Molecular Science Research Hub
Imperial College London
London W12 0BE, UK
E-mail: a.bakulin@imperial.ac.uk
A. C. Yüzer, Prof. M. Ince
Department of Energy Systems Engineering
Faculty of Technology
Tarsus University
Mersin 33400, Turkey
Prof. J. R. Durrant
SPECIFIC
College of Engineering
Swansea University Bay Campus
Swansea SA1 8EN, UK
Prof. K. Vandewal
Institute for Materials Research (IMO-IMOMEC)
Hasselt University
Wetenschapspark 1, Diepenbeek 3590, Belgium
E-mail: koen.vandewal@uhasselt.be
The ORCID identification number(s) for the author(s) of this article can be found under https://doi.org/10.1002/aenm.202002124.

[+]Present address: Heliatek GmbH, Treidlerstraße 3, 01139 Dresden, Germany

DOI: 10.1002/aenm.202002124

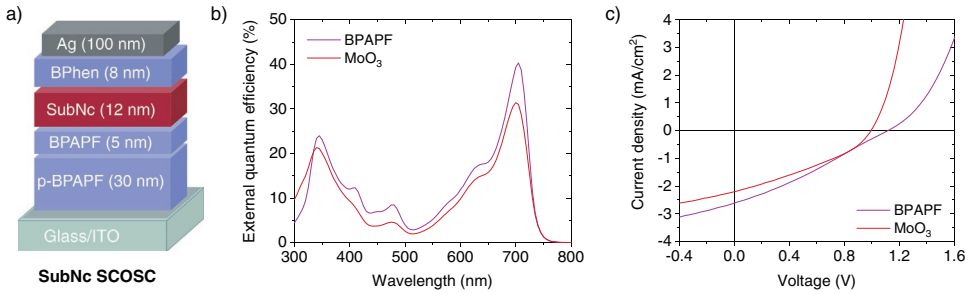

Figure 1. a) Device architecture of the investigated single-component organic solar cells (SCOSC) employing SubNc as the only photo-active material and BPAPF as hole transport layer. A device with MoO_3 is also included for comparison. The full device structures can be found in Experimental Section. b) External quantum efficiency (EQE) spectra demonstrating the high EQEs observed in the SubNc SCOSCs, despite the absence of an acceptor material. c) Current–voltage characteristic curves of the investigated devices.

meaning that the HOMOs and lowest unoccupied molecular orbitals (LUMOs) are aligned in a staggered way.[19] It remains, therefore, a question as to why these devices still generate photocurrent efficiently.

In this work, we investigate the origin of charge photo-generation in SubNc based devices. Using transient absorption (TA) spectroscopy measurements, we confirm that the observed high EQEs in these devices are not due to a hidden charge-generating interface between SubNc and transport layers or contacts. Moreover, we observe that charge generation is only present when SubNc is sandwiched between electrodes, but not for pristine SubNc thin films on glass, indicating that it is a field-assisted effect. As a counterexample, we find that the small molecule DBP does not exhibit this effect. In order to probe the consequence in D–A solar cells, we prepared bilayer devices incorporating either DBP or SubNc combined with a series of chloroboron subphthalocyanine (SubPc) derivatives with various degrees of chlorination as acceptors. The series of SubPc derivatives offers an ideal testbed for elucidating the field effect on charge generation in small molecule materials systems with various driving forces for charge separation, enabling driving forces varying from about 0.38 eV down to values close to (or below) the thermal energy at room temperature. We show that in contrast to DBP, field-assisted generation in SubNc leads to high internal quantum efficiencies of 80% and EQEs of 70% which remain unaffected as the driving force is minimized. This leads to a suppression of voltage losses from 0.89 V down to 0.57 V, while keeping the photocurrent high. This work demonstrates that field-assisted charge generation can be efficient in certain neat organic semiconductors and can be used to combine low voltage losses with high quantum efficiencies in OSCs.

2. Results and Discussion

2.1. High EQE in SubNc Based Single-Component Organic Solar Cells

In the investigated SCOSCs, SubNc is inserted between ITO and Ag contacts, together with electron and hole transport layers (ETL and HTL, respectively), which improve the contact selectivity and device performance (**Figure 1**a).[20–22] Bathophenanthroline (BPhen) is used as ETL, and 9,9-bis[4-(*N*,*N*-bis-biphenyl-4-yl-amino)phenyl]-9H-fluorene (BPAPF) is used as HTL. BPAPF was selected as it showed the best performance among various HTL materials (Figure S1, Supporting Information), whose HOMO is in the range of that of SubNc (Table S1, Supporting Information). As shown in Figure 1a, a thin (5 nm) layer of intrinsic BPAPF is used next to SubNc as exciton blocking layer, and a thicker layer (30 nm) of doped BPAPF (p-BPAPF) is placed on ITO to ensure lossless hole transport.[20] MoO_3 was originally used in the work of Chandran et al., and a similar device was also included in this work, for comparison. Further details about the device structure can be found in the Experimental Section.

The best device performance is achieved when using BPAPF with a peak EQE reaching 40% (Figure 1b), and a short-circuit current density (J_{SC}) of almost 3 mA cm^{-2}, although the fill-factor (FF) is still low (Figure 1c). The open-circuit voltage (V_{OC}) is equal to 1.12 V, which is rather high as compared to the optical gap (E_{opt}) of SubNc of 1.73 eV.[23,24] In addition to this, we do not observe any subgap absorption features in the sensitively measured EQE spectra which could be attributed to the formation of CT states at the BPAPF/SubNc interface (Figure S2, Supporting Information). This implies that the investigated device indeed operates as OSC even though no low energy charge-generating interface is present.

2.2. Field-Assisted Free Charge Generation in SubNc Based Single-Component Organic Solar Cells

To elucidate the charge generation mechanism in the SubNc based SCOSC, we employed TA spectroscopy on the SCOSC using BPAPF, as well as pristine SubNc films on glass. As shown in **Figure 2**a,b, strong ground-state bleaching (GSB) signals around 700 nm are observed in both samples, immediately after photoexcitation. Additionally, the photoinduced absorption (PIA) arises immediately in the region between 725 and 800 nm. Interestingly, the GSB peak shifts to shorter wavelengths in the film whereas it shifts to a longer wavelength in the device at longer pump-probe time delays. This indicates that the photoinduced species at long times (1–5 ns) differ in the film from that in the device, although the initially photoinduced species are the same. Besides being related to

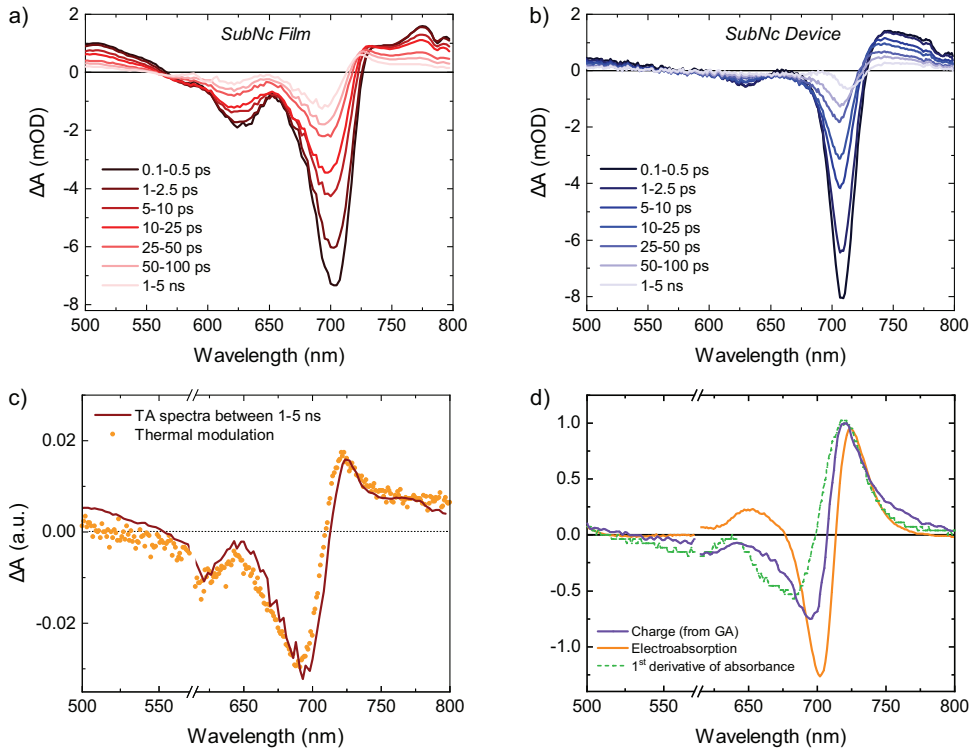

Figure 2. Spectroscopy characterization of SubNc thin films and devices. a) and b) transient absorption (TA) spectra for the SubNc thin film and SCOSC, respectively. c) Comparison of the TA spectra between 1–5 ns in the SubNc thin film with the thermal modulation signal obtained from the differential absorbance spectra at various temperatures as indicated in Figure S3, Supporting Information. d) For SubNc SCOSC, comparing the electroabsorption (EA) spectra with the first derivative of SubNc absorbance spectra and the spectra for charge (decomposed from global analysis).

the conversion of excitons into charges, the peak shift can have several other origins including thermochromic shifts. To thoroughly understand the origin of the GSB peak shift, SubNc films were heated to various temperatures and the in-situ change in the absorbance was characterized by UV–Vis absorption spectroscopy. Figure S3, Supporting Information, shows that the absorbance decreases as temperature increases.[25] The difference in the absorbance spectrum between the high temperature and the low temperature giving the thermal modulation signal is shown in Figure 2c. This spectrum resembles the shape of the TA spectra for the film between 1–5 ns, hence we conclude that the GSB peak shift in the film is due to the slow arousal of the thermal modulation signal, but not due to charge generation. The origin of thermal modulation signals in organic semiconductors has usually been attributed to the reduction in the effective conjugation length as a result of the thermally induced dynamic disorder, but it can also be related to thermally assisted population of subgap states.[26–29] In either case, it is not suggesting any charge generation in the film. Moving to the device, the TA spectra between 1–5 ns differs considerably from the thermal modulation signal as shown in Figure S4, Supporting Information. In fact, it resembles the electroabsorption (EA) spectra (Figure 2d) measured independently for a SubNc based SCOSC. Furthermore, using a global analysis based on genetic algorithm which decouples the individual dynamics for each species (Figure S5, Supporting Information), it is shown that both the exciton and the EA gradually decay followed by charge generation at the same time. Moreover, the instantaneous rise of the kinetics for both charge and EA suggests that a portion of the charges is already generated within sub-ps. This confirms that charge generation is occurring much more efficiently in the device than in neat films on glass. In summary, the majority of excitons undergo relaxation and dissipate to heat in SubNc thin films on glass, without electrodes. On the contrary, the thermal modulation disappears as a result of the efficient conversion from excitons to charges in the SubNc device.

To elucidate the impact of other interfaces on the charge generation in the SubNc based SCOSC with BPAPF, further photoluminescence (PL) and TA measurements were carried out on a series of bilayer films on glass with SubNc and every other layer existing in the device (ITO, p-doped BPAPF, BPAPF, BPhen). As shown in Figure S6, Supporting Information, the PL quenching is minimum and negligible regardless of the type of interface present. Moreover, the same exciton decay lifetime is observed in all the samples, which indicates that charge generation in the SCOSC is not assisted by any interfacial quenching (Figure S7, Supporting Information), thus excluding also the case of charge generation due to energy level electrostatic shifts within the bulk of neat SubNc or at an interface between SubNc and another material in the device.[30,31] Finally, we conclude that charge generation in SubNc based SCOSCs occurs only when both electrodes are present and, thus, attribute it to the presence of the built-in electric field in the device, which arises from the work function difference of the metal electrodes.

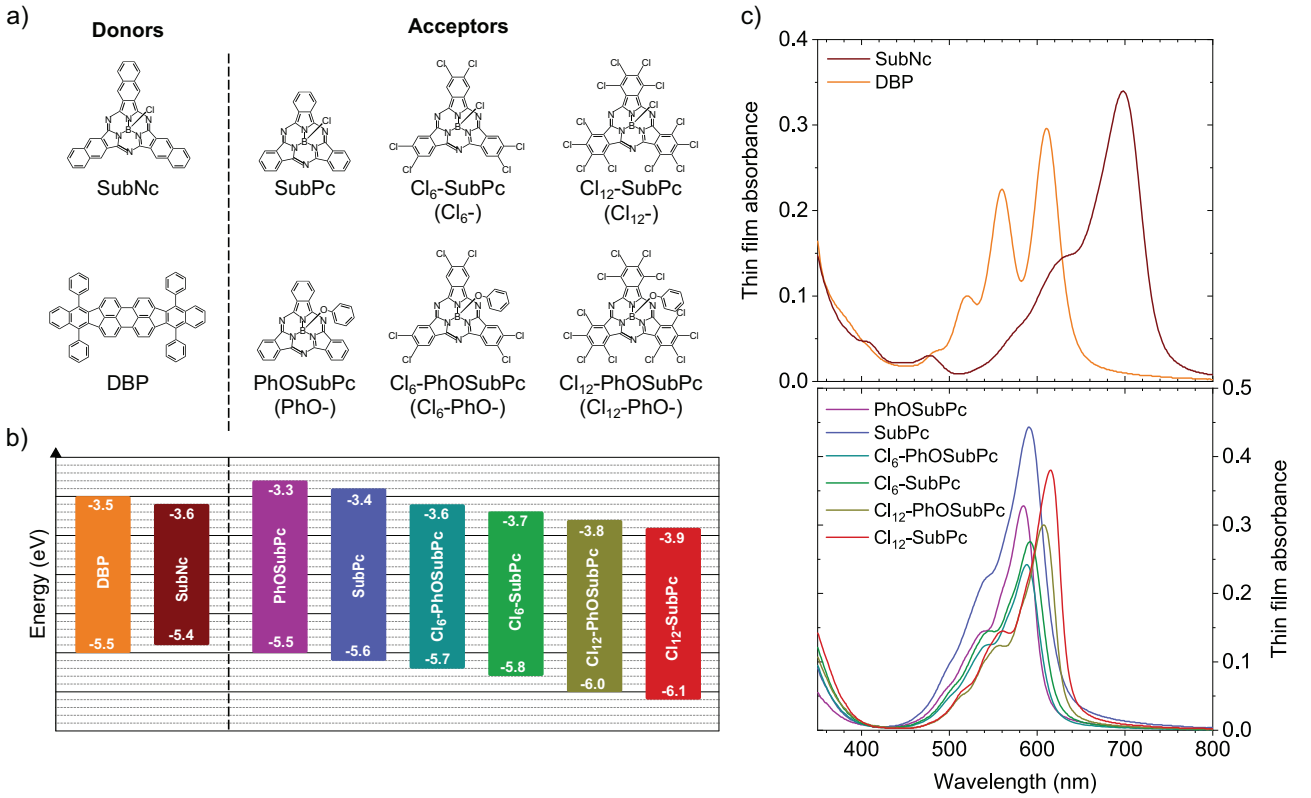

Figure 3. a) Chemical structures of the materials used to fabricate the investigated bilayer solar cells. b) Energy levels of DBP, SubNc, and SubPc derivatives, measured with cyclic voltammetry and taken from literature.[35–39] c) UV–Vis absorbance for thin films of SubNc (12 nm) and DBP (15 nm) (top panel) and SubPc derivatives (15 nm) (bottom panel).

2.3. Constant and Driving-Force-Independent IQE in SubNc-Based OSCs

Having shown that charge generation in neat SubNc can be efficient in the presence of an electric field, we now move on to study the impact of this effect on classical D–A heterojunction devices. We built OSCs employing SubNc or DBP as donors, with a set of peripherally and axially substituted chloroboron subphthalocyanines (SubPc) as acceptors. DBP is selected as a representative example of an organic semiconductor, where the generation of charges in the neat material occurs at a very low efficiency, even in the presence of an electrical field. This is deduced from its rather poor performance in SCOSCs, demonstrating EQEs that hardly reach 2% and a PCE of 0.1%, as shown in Figure S8, Supporting Information. The set of SubPc derivatives used here as acceptors consists of six different compounds having twelve (Cl_{12}), six (Cl_6), or no chlorine atoms in the periphery. For each chlorination degree, we have a derivative with either a chlorine (Cl) atom or a phenoxy (PhO) group in the axial position (**Figure 3**a). The different chlorination degrees result in different energetics: substitution of the chlorine atom in the axial position of SubPc with a phenoxy group increases the LUMO by approximately 100 meV,[32] while the addition of six chlorine atoms in the periphery of the molecule reduces the LUMO by 300 meV.[33,34] All these variations lead to a set of acceptors with LUMOs spanning from −3.3 to −3.9 eV (Figure 3b), without altering their E_{opt} (Figure 3c), enabling a large tunability of the driving force between D and A, and hence the E_{CT} at the interface with either SubNc or DBP.[35–39]

From Figure 3b, it is immediately clear that several material combinations cannot lead to a charge generating type-II heterojunction. The energy levels of PhOSubPc and SubPc exceed those of SubNc, which results in the absence of subgap absorption features related to CT states in the devices sensitive EQE spectra (**Figure 4**a). The same is valid for the DBP/PhO-SubPc and DBP/SubPc devices, since the HOMO and LUMO of PhOSubPc and SubPc are close to those of DBP (Figure 4d). This leads to current–voltage curves that are strongly s-kinked, exhibiting poor FFs (Figure 4 and Table S2, Supporting Information). For all the other devices with Cl_6– or Cl_{12}– SubPc derivatives, we observe redshifted weak absorption shoulders related to CT states in the EQE spectra of the DBP/acceptor and SubNc/acceptor solar cells (Figure 4a,d). By Gaussian fitting the CT state absorption features and the singlet exciton peak at the low-energy edge of the sEQE spectra (Figures S9 and S10, Supporting Information), we are able to extract the values for E_{CT} and E_{opt} and, hence, the driving force (i.e., E_{opt}–E_{CT}) for each device (Table S3, Supporting Information).[40,41]

All EQE spectra of the SubNc-based devices look very similar (Figure 4a), with the EQE peak at 705 nm (corresponding to the absorption peak of SubNc) being almost always equal at 70%, regardless of the energy levels of the used acceptor. The EQE of 70% occurs even in the SubNc/PhOSubPc and SubNc/SubPc devices, which are not expected to form a type-II heterojunction.

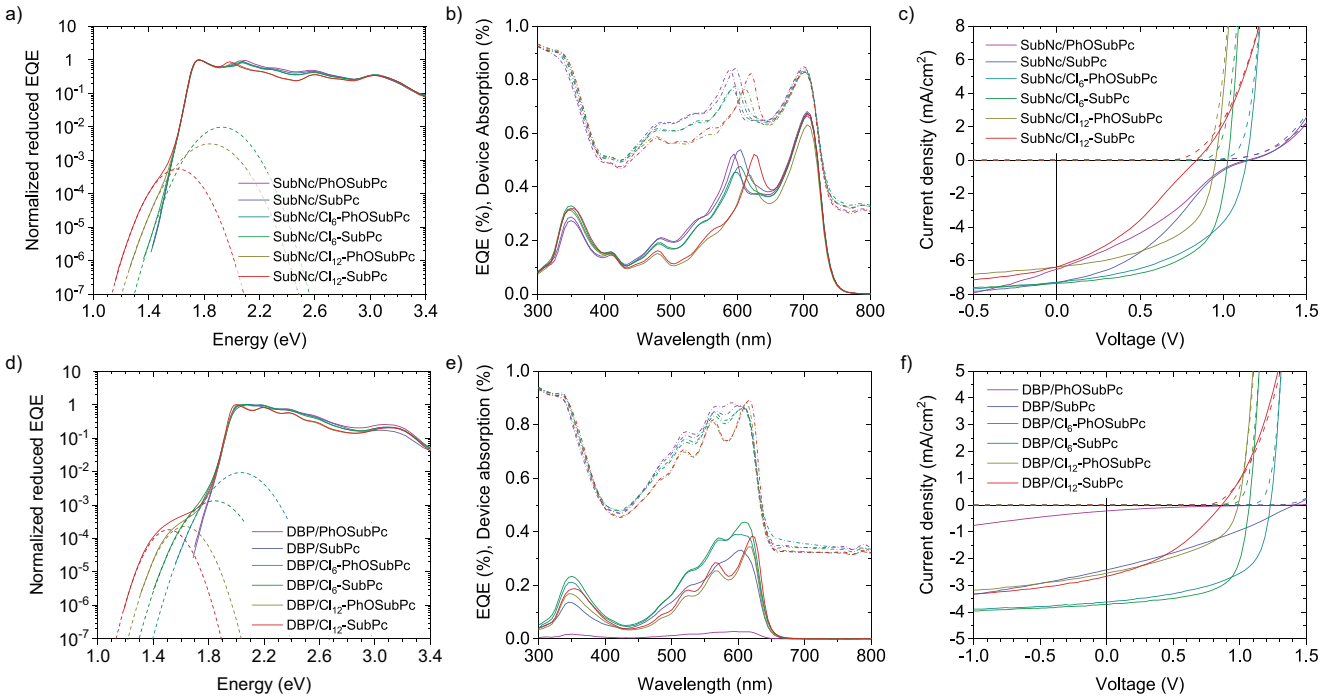

Figure 4. EQE and current–voltage characteristics of the investigated devices comprising SubNc and DBP as donors, and six different SubPc derivatives as acceptors. Sensitively measured EQE spectra showing the formation of (Gaussian fitted, dashed lines) CT states, redshifting as the driving force increases, for the devices based in a) SubNc and d) DBP. EQE spectra in linear scale (solid lines) and device absorption (dashed lines, taken as 1–*R* where *R* is the device reflection) for the b) SubNc and e) DBP devices, respectively. c,f) Current–voltage characteristic curves for the investigated devices under 1 sun illumination (solid lines) and in dark (dashed lines).

This leads to a J_{SC} which remains at around 7 mA cm^{-2} and independent on the driving force at the SubNc/acceptor interface (**Figure 5**a), thus demonstrating the beneficial effects of field-assisted charge generation in the SubNc-based devices. It is worth noting that J_{SC} and FF depend on the field strength, since a stronger built-in field improves charge extraction.[42] Moreover, the J_{SC} would improve if the SubNc and SubPc derivatives could be replaced by materials with a broader absorption spectrum, also covering the 350 to 550 nm wavelength range, where SubNc and SubPc absorption is weak. On the other hand, in the case of the DBP/PhOSubPc solar cell with minimal driving force, the EQE does not exceed 2%. A strong dependence of EQE and J_{SC} is observed on the driving force, in the DBP/acceptor solar cells (Figures 4b and 5a). J_{SC} starts small (0.2 and 2.4 mA cm^{-2} for the DBP/PhOSubPc and DBP/SubPc) and increases (up to 3.7 mA cm^{-2}) in the devices with the hexachlorinated SubPc derivatives (Cl_6— and Cl_6—PhO—) showing a mid-range driving force of 291 and 443 meV, respectively. EQE reduces slightly for the larger driving force (559 and 649 meV) devices with the dodecachlorinated derivatives (Cl_{12}— and Cl_{12}—PhO—). In these devices, the drop in J_{SC} and the FF (Figure 5a,c), could be due to the reduced effective gap between D and A that can lead to faster recombination rates, affecting the free charge carrier generation and extraction and providing the message that high driving forces do not necessarily lead to the highest photocurrents.[43]

In the case of the DBP based devices, we observe a clear trade-off between photocurrent and photovoltage: J_{SC} increases with driving force, but V_{OC} is maximized (1.42 V) when the driving force is close to (or less than) k_BT (Figure 5b). However, the SubNc based solar cells show a constant photocurrent generation efficiency as their V_{OC} increases and, hence, the total energy losses (E_{opt}–qV_{OC}) decrease (Figure 5e). Since the absorption at the SubNc peak is not affected by the acceptor, the constant EQE of 70% is the result of a constant internal quantum efficiency (IQE_{dev}) of more than 80% over the whole driving force range(Figure 4b). This demonstrates that field-assisted charge generation helps low offset D–A combinations with high open-circuit voltages achieve a higher internal quantum efficiency and, thus, overall power conversion efficiency. IQE_{dev} is obtained by comparing the EQE peaks to the absorption of the total device obtained via reflectance measurements at the same wavelength (Figure 4b).[44] In total, the E_{opt}–qV_{OC} losses of the investigated SubNc based devices reduce by 0.32 eV, reaching 0.57 eV for the SubNc/SubPc device (Table S3, Supporting Information). In addition to reducing the voltage losses directly, the reduction of the driving force also results in an increase of the device's external quantum efficiency of electroluminescence (EQE_{EL}), leading to a reduction of the non-radiative voltage losses (ΔV_{nonrad}).[12] In the SubNc based devices, we managed to increase their EQE_{EL} by almost two orders of magnitude, without losing photocurrent (Figure 5d and Table S4, Supporting Information). This increase of EQE_{EL} corresponds to a reduction of ΔV_{nonrad} losses of approximately 145 mV, reaching a value of 173 meV for the SubNc/SubPc cell which is among the low ones reported for OSCs with a low E_{opt} of 1.73 eV.[45–48]

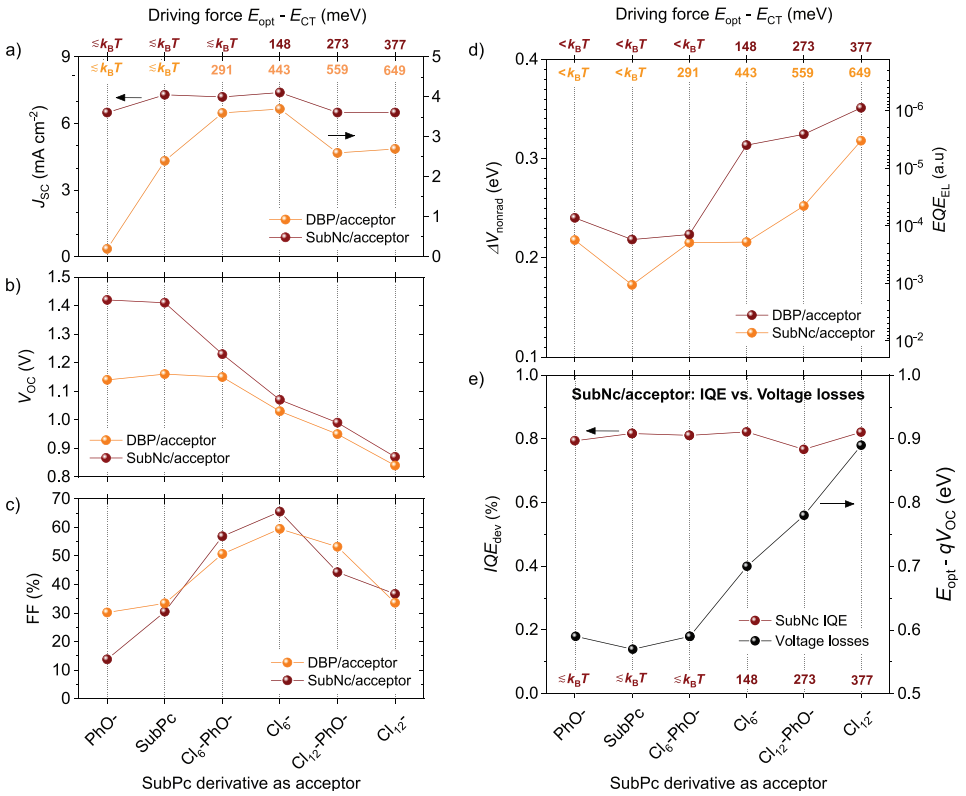

Figure 5. Photovoltaic parameters and voltage losses as a function of driving force. a) Short-circuit current density (J_{SC}), b) open-circuit voltage (V_{OC}), and c) fill-factor (FF) for D–A organic solar cells based on SubNc (red) and DBP (orange), and six SubPc derivatives with different degrees of chlorination used as acceptors, leading to different driving forces in each case (colored numbers on top axis, red for SubNc, and orange for DBP). d) Non-radiative voltage losses (ΔV_{nonrad}) as a function of the driving force for both SubNc/acceptor and DBP/acceptor solar cells, showing an increase in external quantum efficiency of electroluminescence (EQE_{EL}) and a decrease in ΔV_{nonrad}, as the driving force is minimized. e) Internal quantum efficiency of the complete device (IQE_{dev}) and total energy losses for the SubNc/acceptor devices where the field-assisted charge generation results in constant IQE_{dev} as the driving force is minimized and the energy losses reduced. IQE_{dev} is calculated at the SubNc peak wavelength (705 nm) as IQE_{dev} = EQE/1–R, both EQE and 1–R are shown in Figure 4b.

3. Conclusions

In this work, we investigate the free charge carrier generation upon illumination in neat SubNc thin films and SubNc layers sandwiched between selective electrodes. Only in the latter case we observe the generation of a significant density of charges upon photo-excitation, leading to the conclusion that free carrier generation is field-assisted and due to the built-in potential of the SubNc based devices. We show that field-assisted charge generation can be used to minimize the trade-off between photocurrent and photovoltage. Using SubNc as a donor combined with a series of SubPc derivatives as acceptors with various driving forces, we achieve constantly high quantum efficiencies even in devices with a negligible driving force, where voltage losses due to charge transfer and non-radiative recombination are minimized. This stands in stark contrast to the situation when DBP is used as donor, where no field-assisted charge generation on the neat material occurs and a pronounced dependence of the photocurrent on driving force is observed. The case of SubNc devices, therefore, demonstrates a new paradigm in the design of organic photovoltaic materials and systems, where charge generation can be facilitated in neat materials with no additional voltage losses related to heterointerfaces.

4. Experimental Section

Device Fabrication: The solar cells were processed by thermal evaporation in a custom-made vacuum system (Kurt J. Lesker, USA) with a base pressure of 10^{-7} mbar. During a processing run, different masks and movable shutters enabled the variation of the device stacks or processing parameters, offering the possibility to produce and compare various devices at the same processing conditions. Each device was fabricated onto either clean glass substrates or substrates with pre-structured ITO (Thin Film Devices, USA), which underwent an ozone treatment for cleaning before being transferred into the vacuum chamber. Every investigated device was bottom illuminated, employing thin Ag or indium tin oxide (ITO) as anode and a 100 nm thick Ag cathode. The area of the devices was 6.44 mm^2, defined as the overlap between anode and the Ag cathode. All the used materials were purified twice in-house by vacuum gradient sublimation. The solar cells were encapsulated in nitrogen atmosphere with a transparent encapsulation glass, fixed by UV-hardened epoxy glue.

Device Structures: Hole transporting layer (HTL) materials such as BF-DPB (Synthon, Germany), BPAPF (Lumtec, Taiwan), and α-NPD (Lumtec, Taiwan) were p-doped by NDP9 (Novaled, Germany), at a 10 wt% mixing ratio. A 30-nm-thick doped HTL (p-HTL) was deposited on top of the anode (ITO). In each case, an intrinsic layer of 5 nm thickness of the used HTL was used as exciton blocking layer, avoiding also the contact between the active layer and the p-dopant. In the active layer, 12 nm of SubNc (Lumtec, Taiwan) or 15 nm of DBP (synthesized in-house) were used as donors, and 18 nm of PhOSubPc (synthesized in-house),

or SubPc (Lumtec, Taiwan), or Cl_6-PhOSubPc (Lumtec, Taiwan), Cl_6-SubPc (Lumtec, Taiwan), or Cl_{12}-PhOSubPc (synthesis procedure in SI), or Cl_{12}-SubPc (synthesis procedure in SI) were used as acceptors. Donor and acceptor layers were sequentially deposited forming a planar heterojunction. In the devices, 8 nm of BPhen (ABCR, Germany) were used as exciton blocking and electron transporting layer. For the single-component organic solar cells (SCOSCs), the acceptor layer was skipped and the other layers (and the thicknesses) remain the same as described above. In the case of the SubNc based SCOSC with MoO_3, 3 nm of MoO_3 replace both the intrinsic and doped HTL, so that SubNc in deposited directly on MoO_3. Each organic material was evaporated at a rate of 0.3 Å s^{-1}, apart from SubNc and Cl_6-PhOSubPc which were deposited at 0.5 Å s^{-1}. The Ag electrodes were deposited at 1 Å s^{-1}. All layer thicknesses were monitored with calibrated quartz crystal microbalances. All thin film samples on glass or ITO shown in this work reproduce the layers in the solar cells as described above, regarding deposition conditions and layer thicknesses. Long names of the materials used in this work: 9,9-bis[4-(*N,N*-bis-biphenyl-4-yl-amino)phenyl]-9H-fluorene (BPAPF), *N,N′*-diphenyl-*N,N′*-bis(9,9-dimethyl-fluorene-2-yl)-benzidine (BF-DPB), 2,2′-Dimethyl-*N,N′*-di-[(1-naphthyl)-*N,N′*-diphenyl]-1,1′-biphenyl-4,4′-diamine (α-NPD), tetraphenyldibenzoperiflanthene (DBP), and molybdenum trioxide (MoO_3).

Current Voltage (J–V) Measurements: *J–V* measurements were carried out in ambient conditions using a source measurement unit (SMU 2400 Keithley, USA) and a simulated AM1.5G illumination (16S-003-300-AM1.5G sunlight simulator, Solar Light Co., USA). A silicon photodiode (Hamamatsu S1337) was used as reference. Spectral mismatch was taken into account during the measurement.

External Quantum Efficiency (EQE) Measurements: EQE measurements were performed using a xenon lamp (Oriel Xe Arch-lamp Apex, Newport, USA), a monochromator (Cornerstone 260 1/4m, Newport, USA), an optical chopper, and a lock-in amplifier (SR 7265, Signal Recovery, USA). The EQE of the OSCs was measured with an aperture mask (2.78 mm^2) and without bias light. A calibrated silicon photodiode (Hamamatsu S1337, Japan) was used as reference.

Sensitive EQE Measurements: The light of a quartz halogen lamp (50 W) was chopped at 140 Hz and coupled into a monochromator (Newport Cornerstone 260 1/4m, USA). The resulting monochromatic light was focused onto the OSC, its current at short-circuit conditions was fed to a current pre-amplifier before it was analyzed with a lock-in amplifier (Signal Recovery 7280 DSP, USA). The time constant of the lock-in amplifier was chosen to be 500 ms and the amplification of the pre-amplifier was increased to resolve low photocurrents. The EQE was determined by dividing the photocurrent of the OSC by the flux of incoming photons, which was obtained with calibrated silicon (Si) and indium-gallium-arsenide (InGaAs) photodiodes.

Electroluminescence Measurements: Electroluminescence (EL) spectra were acquired with an Andor SR393i-B spectrometer equipped with an iDus silicon (DU420A-BR-DD) and an InGaAs (DU491A-1.7) detector array. The spectral response of the setup (detector and grating) was evaluated by means of a calibrated lamp (Oriel 63355). The EL spectra were acquired by driving the solar cells with a Keithley 2400 SMU at injection currents equivalent to their short-circuit current.

Photoluminescence Measurements: Photoluminescence spectra were measured with a Fluorolog-3 spectrofluorometer (FL3-22, Horiba Jobin Yvon). Measurements were carried out in a front-face geometry where the samples were excited at 600 nm.

Transient Absorption Spectroscopy: Transient absorption spectra were acquired using a Ti-sapphire regenerative amplifier (Solstice, Spectra Physics) which seeds pulses of 800 nm at 1 kHz repetition rate. One part of the pulses was sent to an optical parametric amplifier (TOPAS, Light conversion) followed by a frequency mixer (NirUVis, Light conversion) to generate tunable wavelengths as the visible pump pulse (700 nm for the experiments in this paper). The second part of the 800 nm pulses was sent to a mechanical delay stage and then through a non-linear crystal to generate supercontinuum which acts as the probe pulse with a spectral range of 350 to 1600 nm. Both pump and probe pulses were then sent through HELIOS femtosecond transient absorption spectrometer setup (Ultrafast Systems) and focused onto a 0.5 mm^2 spot on the samples. SubNc based solar cells were measured with a reflectance set up, exciting the device from the ITO side. A graphical representation of the setup is depicted in Figure S11, Supporting Information.

Global Analysis: Global analysis (GA) was carried out based on a genetic algorithm as detailed elsewhere, a global fitting solution to decouple 2D TA spectra when there are overlapping features.[49] Through random guesses, a number of spectra were generated after inputting the 2D TA. It then evolves to find the best fitness. Through a few repetitions, the 2D TA were decomposed into individual components together with corresponding kinetics.

Supporting Information

Supporting Information is available from the Wiley Online Library or from the author.

Acknowledgements

V.C.N. and Y.D. contributed equally to this work. The authors would like to thank Prof. Dr. Dieter Neher for providing measurement time on the electroluminescence setup of his lab at University of Potsdam. They would also like to acknowledge the Optoelectronics group in the University of Cambridge for sharing the global analysis codes. This work was supported by the German Federal Ministry of Education and Research (BMBF) through the InnoProfile project "Organische p-i-n Bauelemente2.2" (FKZ 03IPT602X). A.A.B. is a Royal Society university research fellow.

Open access funding enabled and organized by Projekt DEAL.

Conflict of Interest

The authors declare no conflict of interest.

Keywords

charge generation, driving force, field-dependent, organic solar cells, ultrafast spectroscopy

Received: June 29, 2020
Revised: September 23, 2020
Published online: November 9, 2020

[1] C. W. Tang, *Appl. Phys. Lett.* **1986**, *48*, 183.
[2] S. D. Dimitrov, J. R. Durrant, *Chem. Mater.* **2014**, *26*, 616.
[3] K. Vandewal, *Annu. Rev. Phys. Chem.* **2016**, *67*, 113.
[4] T. Ferron, M. Waldrip, M. Pope, B. A. Collins, *J. Mater. Chem. A* **2019**, *7*, 4536.
[5] S. Few, J. M. Frost, J. Nelson, *Phys. Chem. Chem. Phys.* **2015**, *17*, 2311.
[6] S. Cook, R. Katoh, A. Furube, *J. Phys. Chem. C* **2009**, *113*, 2547.
[7] J. Liu, S. Chen, D. Qian, B. Gautam, G. Yang, J. Zhao, J. Bergqvist, F. Zhang, W. Ma, H. Ade, O. Inganäs, K. Gundogdu, F. Gao, H. Yan, *Nat. Energy* **2016**, *1*, 16089.
[8] K. Nakano, Y. Chen, B. Xiao, W. Han, J. Huang, H. Yoshida, E. Zhou, K. Tajima, *Nat. Commun.* **2019**, *10*, 2520.
[9] B. Gao, H. Yao, L. Hong, J. Hou, *Chin. J. Chem.* **2019**, *37*, 1153.
[10] C. Yang, J. Zhang, N. Liang, H. Yao, Z. Wei, C. He, X. Yuan, J. Hou, *J. Mater. Chem. A* **2019**, *7*, 18889.
[11] Y. Zhong, M. Causa, G. J. Moore, P. Krauspe, B. Xiao, F. Günther, J. Kublitski, R. Shivhare, J. Benduhn, E. BarOr, S. Mukherjee,

K. M. Yallum, J. Réhault, S. C. B. Mannsfeld, D. Neher, L. J. Richter, D. M. DeLongchamp, F. Ortmann, K. Vandewal, E. Zhou, N. Banerji, *Nat. Commun.* **2020**, *11*, 833.
[12] D. Qian, Z. Zheng, H. Yao, W. Tress, T. R. Hopper, S. Chen, S. Li, J. Liu, S. Chen, J. Zhang, X. K. Liu, B. Gao, L. Ouyang, Y. Jin, G. Pozina, I. A. Buyanova, W. M. Chen, O. Inganäs, V. Coropceanu, J. L. Bredas, H. Yan, J. Hou, F. Zhang, A. A. Bakulin, F. Gao, *Nat. Mater.* **2018**, *17*, 703.
[13] A. Weu, T. R. Hopper, V. Lami, J. A. Kreß, A. A. Bakulin, Y. Vaynzof, *Chem. Mater.* **2018**, *30*, 2660.
[14] S. N. Hood, I. Kassal, *J. Phys. Chem. Lett.* **2016**, *7*, 4495.
[15] J. Roncali, I. Grosu, *Adv. Sci.* **2019**, *6*, 1801026.
[16] N. Cho, C. W. Schlenker, K. M. Knesting, P. Koelsch, H. L. Yip, D. S. Ginger, A. K. Y. Jen, *Adv. Energy Mater.* **2014**, *26*, 6125.
[17] T. Hahn, S. Tscheuschner, C. Saller, P. Strohriegl, P. Boregowda, T. Mukhopadhyay, S. Patil, D. Neher, H. Bässler, A. Köhler, *J. Phys. Chem. C* **2016**, *120*, 25083.
[18] V. D. Mitchell, D. J. Jones, *Polym. Chem.* **2018**, *9*, 795.
[19] H. T. Chandran, T. W. Ng, Y. Foo, H. W. Li, J. Qing, X. K. Liu, C. Y. Chan, F. L. Wong, J. A. Zapien, S. W. Tsang, M. F. Lo, C. S. Lee, *Adv. Mater.* **2017**, *29*, 1606909.
[20] B. Maennig, J. Drechsel, D. Gebeyehu, P. Simon, F. Kozlowski, A. Werner, F. Li, S. Grundmann, S. Sonntag, M. Koch, K. Leo, M. Pfeiffer, H. Hoppe, D. Meissner, N. S. Sariciftci, I. Riedel, V. Dyakonov, J. Parisi, *Appl. Phys. A: Mater. Sci. Process.* **2004**, *79*, 1.
[21] Z. Yin, J. Wei, Q. Zheng, *Adv. Sci.* **2016**, *3*, 1500362.
[22] K. Walzer, B. Maennig, M. Pfeiffer, K. Leo, *Cell* **2007**, *107*, 1233.
[23] V. C. Nikolis, J. Benduhn, F. Holzmueller, F. Piersimoni, M. Lau, O. Zeika, D. Neher, C. Koerner, D. Spoltore, K. Vandewal, *Adv. Energy Mater.* **2017**, *7*, 1700855.
[24] V. C. Nikolis, A. Mischok, B. Siegmund, J. Kublitski, X. Jia, J. Benduhn, U. Hörmann, D. Neher, M. C. Gather, D. Spoltore, K. Vandewal, *Nat. Commun.* **2019**, *10*, 3706.
[25] A. Rao, M. W. B. Wilson, S. Albert-Seifried, R. D. i. Pietro, R. H. Friend, *Phys. Rev. B* **2011**, *84*, 195411.
[26] S. D. Jung, D. H. Hwang, T. Zyung, W. H. Kim, K. G. Chittibabu, S. K. Tripathy, *Synth. Met.* **1998**, *98*, 107.
[27] F. A. C. Oliveira, L. A. Cury, A. Righi, R. L. Moreira, P. S. S. Guimarães, F. M. Matinaga, M. A. Pimenta, R. A. Nogueira, *J. Chem. Phys.* **2003**, *119*, 9777.
[28] A. Rao, M. W. B. Wilson, S. Albert-Seifried, R. D. I. Pietro, R. H. Friend, *Phys. Rev. B* **2011**, *84*, 195411.
[29] S. Selim, E. Pastor, M. García-Tecedor, M. R. Morris, L. Francàs, M. Sachs, B. Moss, S. Corby, C. A. Mesa, S. Gimenez, A. Kafizas, A. A. Bakulin, J. R. Durrant, *J. Am. Chem. Soc.* **2019**, *141*, 18791.
[30] Y. Dong, V. C. Nikolis, F. Talnack, Y.-C. Chin, J. Benduhn, G. Londi, J. Kublitski, X. Zheng, S. C. B. Mannsfeld, D. Spoltore, L. Muccioli, J. Li, X. Blase, D. Beljonne, J.-S. Kim, A. A. Bakulin, G. D'Avino, J. R. Durrant, K. Vandewal, *Nat. Commun.* **2020**, *11*, 4617.
[31] M. Schwarze, K. S. Schellhammer, K. Ortstein, J. Benduhn, C. Gaul, A. Hinderhofer, L. Perdigón Toro, R. Scholz, J. Kublitski, S. Roland, M. Lau, C. Poelking, D. Andrienko, G. Cuniberti, F. Schreiber, D. Neher, K. Vandewal, F. Ortmann, K. Leo, *Nat. Commun.* **2019**, *10*, 2466.
[32] C. Duan, G. Zango, M. G. Iglesias, F. J. M. Colberts, M. M. Wienk, M. V. Martínez-Díaz, R. A. J. Janssen, T. Torres, *Angew. Chem., Int. Ed.* **2016**, *1*, 154.
[33] C. G. Claessens, D. González-Rodríguez, M. S. Rodríguez-Morgade, A. Medina, T. Torres, *Chem. Rev.* **2014**, *114*, 2192.
[34] G. E. Morse, T. P. Bender, *ACS Appl. Mater. Interfaces* **2012**, *4*, 5055.
[35] G. E. Morse, M. G. Helander, J. Stanwick, J. M. Sauks, A. S. Paton, Z. H. Lu, T. P. Bender, *J. Phys. Chem. C* **2011**, *115*, 11709.
[36] P. Sullivan, A. Duraud, L. Hancox, N. Beaumont, G. Mirri, J. H. R. Tucker, R. A. Hatton, M. Shipman, T. S. Jones, *Adv. Energy Mater.* **2011**, *1*, 352.
[37] J. S. Castrucci, D. S. Josey, E. Thibau, Z.-H. Lu, T. P. Bender, *J. Phys. Chem. Lett.* **2015**, *6*, 3121.
[38] Z. Wang, D. Yokoyama, X.-F. Wang, Z. Hong, Y. Yang, J. Kido, *Energy Environ. Sci.* **2013**, *6*, 249.
[39] A. Barito, M. E. Sykes, B. Huang, D. Bilby, B. Frieberg, J. Kim, P. F. Green, M. Shtein, *Adv. Energy Mater.* **2014**, *4*, 1400216.
[40] K. Vandewal, J. Benduhn, V. C. Nikolis, *Sustainable Energy Fuels* **2018**, *2*, 538.
[41] K. Vandewal, S. Mertens, J. Benduhn, Q. Liu, *J. Phys. Chem. Lett.* **2020**, *11*, 129.
[42] E. Siebert-Henze, V. G. Lyssenko, J. Fischer, M. Tietze, R. Brueckner, T. Menke, K. Leo, M. Riede, *Org. Electron.* **2014**, *15*, 563.
[43] E. Collado-Fregoso, S. N. Pugliese, M. Wojcik, J. Benduhn, E. Bar-Or, L. Perdigón Toro, U. Hörmann, D. Spoltore, K. Vandewal, J. M. Hodgkiss, D. Neher, *J. Am. Chem. Soc.* **2019**, *141*, 2329.
[44] A. Armin, M. Velusamy, P. Wolfer, Y. Zhang, P. L. Burn, P. Meredith, A. Pivrikas, *ACS Photonics* **2014**, *1*, 173.
[45] J. Benduhn, K. Tvingstedt, F. Piersimoni, S. Ullbrich, Y. Fan, M. Tropiano, K. A. McGarry, O. Zeika, M. K. Riede, C. J. Douglas, S. Barlow, S. R. Marder, D. Neher, D. Spoltore, K. Vandewal, *Nat. Energy* **2017**, *2*, 17053.
[46] F. D. Eisner, M. Azzouzi, Z. Fei, X. Hou, T. D. Anthopoulos, T. J. S. Dennis, M. Heeney, J. Nelson, *J. Am. Chem. Soc.* **2019**, *141*, 6362.
[47] S. Ullbrich, J. Benduhn, X. Jia, V. C. Nikolis, K. Tvingstedt, F. Piersimoni, S. Roland, Y. Liu, J. Wu, A. Fischer, D. Neher, S. Reineke, D. Spoltore, K. Vandewal, *Nat. Mater.* **2019**, *18*, 459.
[48] S. Liu, J. Yuan, W. Deng, M. Luo, Y. Xie, Q. Liang, Y. Zou, Z. He, H. Wu, Y. Cao, *Nat. Photonics* **2020**, *14*, 300.
[49] S. Gélinas, O. Paré-Labrosse, C. N. Brosseau, S. Albert-Seifried, C. R. McNeill, K. R. Kirov, I. A. Howard, R. Leonelli, R. H. Friend, C. Silva, *J. Phys. Chem. C* **2011**, *115*, 7114.